Cell Stem Cell
Short Article

Continuous Clonal Labeling Reveals Small Numbers of Functional Stem Cells in Intestinal Crypts and Adenomas

Sarah Kozar,[1,3] Edward Morrissey,[1,3] Anna M. Nicholson,[1] Maartje van der Heijden,[1,2] Heather I. Zecchini,[1] Richard Kemp,[1] Simon Tavaré,[1] Louis Vermeulen,[1,2] and Douglas J. Winton[1,*]
[1]Cancer Research UK Cambridge Institute, University of Cambridge, Li Ka Shing Centre, Robinson Way, Cambridge CB2 0RE, UK
[2]Laboratory for Experimental Oncology and Radiobiology, Center for Experimental Molecular Medicine, Academic Medical Center, Meibergdreef 9, 1105 AZ Amsterdam, The Netherlands
[3]These authors contributed equally to this work
*Correspondence: doug.winton@cruk.cam.ac.uk
http://dx.doi.org/10.1016/j.stem.2013.08.001

SUMMARY

Lineage-tracing approaches, widely used to characterize stem cell populations, rely on the specificity and stability of individual markers for accurate results. We present a method in which genetic labeling in the intestinal epithelium is acquired as a mutation-induced clonal mark during DNA replication. By determining the rate of mutation in vivo and combining this data with the known neutral-drift dynamics that describe intestinal stem cell replacement, we quantify the number of functional stem cells in crypts and adenomas. Contrary to previous reports, we find that significantly lower numbers of "working" stem cells are present in the intestinal epithelium (five to seven per crypt) and in adenomas (nine per gland), and that those stem cells are also replaced at a significantly lower rate. These findings suggest that the bulk of tumor stem cell divisions serve only to replace stem cell loss, with rare clonal victors driving gland repopulation and tumor growth.

INTRODUCTION

Adult stem cells in the intestinal epithelium, as in other tissues, were originally defined by clonogenic assays in which they demonstrated a sustained ability to generate cellular progeny (Siminovitch et al., 1963; Till and McCulloch, 1961; Winton et al., 1988). More recently, endogenous molecular markers have been associated with different subpopulations of intestinal stem cells that demonstrate clonogenicity in genetic-marking experiments, creating much debate about which populations lie ancestrally upstream of others (Barker et al., 2007; Montgomery et al., 2011; Sangiorgi and Capecchi, 2008).

Recent studies have identified significant amounts of overlap of transcriptional and protein profiles in two clonogenic populations in the intestine: the crypt base and suprabasal stem cells, as defined by *Lgr5* and *Hopx/Bmi1* expression, respectively (Itzkovitz et al., 2012; Muñoz et al., 2012). It has also been shown that a bidirectional relationship exists between cells at these locations, suggesting that markers may be inaccurate in identifying the size of the stem cell pool, as they may be lost or others acquired (Takeda et al., 2011). Thus, that all cells defined by marker expression are required for actively maintaining the tissue remains an assumption that has not yet been tested. An alternative possibility is that there is redundancy such that only a proportion of cells sharing a common potentiality actually achieve it.

Similarly, the bulk of evidence for cancer stem cells (CSCs) comes from cell-surface markers that enrich for tumor regrowth on xenotransplantation of disaggregated tumor cells in immunocompromised mice (Shackleton et al., 2009). Such assays may not accurately reflect the native clonogenicity of tumor cells in situ. Moreover, the validity and robustness of CSC markers have been cause for debate (O'Brien et al., 2007; Shmelkov et al., 2008). An alternative and recent approach to validating the CSC concept in mice has been to lineage trace the progeny derived from known stem cell markers such as Lgr5 using intratumoral Cre-mediated recombination (Schepers et al., 2012). This single study in intestinal adenomas has shown that, within a large population of $Lgr5^+$ stem cells, some are clonogenic, and other populations remain untested. Therefore, the size of the clonogenic population acting to maintain the tumor is unknown.

Here, we apply a functional approach independent of stem cell-specific markers. Based on the principle of continuous clonal labeling, it allows the dynamics of clonogenic stem cell replacement to be quantified. This approach exploits the relative instability of dinucleotide repeat tracts during DNA replication by placing a $[CA]_{30}$ tract within a reporter gene. Expression of the reporter gene is only obtained following frameshift mutation. Microsatellite repeats have been used previously to estimate the mitotic age of various tissues in the mouse and have demonstrated the known monoclonality of intestinal crypts; however, the intracrypt dynamics of stem cell replacement have not been addressed using this technique (Reizel et al., 2011). Clonal analysis of human tumors has been restricted to comparing the relatedness of different tumor areas based on changes in methylation patterns (Humphries et al., 2013).

Through analyzing the fate of clones arising during continuous labeling, smaller numbers of stem cells with lower rates of replacement are found to maintain intestinal crypts than has

been indicated previously with stem cell-marker approaches. Subsequent application to intestinal adenomas similarly shows them to be maintained by an unexpectedly small (less than 1%) population characterized by an accelerated rate of stem cell replacement. These results show that adenoma stem cell divisions are inefficient in driving tumor growth and, rather, act to maintain tumor mass via cell turnover.

RESULTS

Formation and Analysis of Clones Arising via Continuous Labeling

To allow ongoing genesis of clones, we placed an out-of-frame *SYNbglA* reporter gene in the Rosa26 housekeeping locus. Expression arose following replication slippage of a $[CA]_{30}$ dinucleotide repeat placed between the translational start site and the remaining coding sequence (Figure 1A). Clones visualized in whole-mount preparations of adult $R26^{[CA]30SYNbglA}$ animals were easily recognized in two ways: first, by migration streams arising from stained crypts and ascending neighboring villi in the small intestine (SI) (Figure 1B); second, as partly or wholly populated crypts in both the SI and colon (Figures 1C and 1D). These clonal patterns are identical to those observed following Cre-mediated "pulse-chase" clone induction and correspond to transition and fixed clonal forms, respectively (Lopez-Garcia et al., 2010; Snippert et al., 2010; Winton and Ponder, 1990).

Adult $R26^{[CA]30SYNbglA}$ mice were aged, and the frequency of wholly and partly populated crypts was determined at three intestinal regions, namely proximal SI, distal SI, and colon. This revealed a linear age-related accumulation of wholly populated crypts up to 759 days (Figures 1E–1G). Notably, the rate of accumulation per 10^5 crypts was higher in the distal SI and colon (2.7 ± 0.5 and 2.8 ± 0.4 per day, respectively) than in the proximal SI (1.0 ± 0.1 per day) (95% confidence interval [CI]). The partly populated, transition-form crypts remain at a constant frequency throughout life but at a level that varied between the different intestinal regions scored (Figures 1E–1G). There are, on average, 132 ± 6, 190 ± 28, and 229 ± 27 (95% CI) partly populated crypts per 10^5 crypts in the proximal SI, distal SI, and colon, respectively. These observations demonstrate that there are regional differences in the rates of clone formation and in the conversion of crypts to monoclonality.

Application of Neutral-Drift Theory to Continuous-Labeling Data

The random process of neutral drift, whereby transition-form crypts resolve to monoclonality, is known to arise from a mode of symmetric stem cell replacement that allows clones to expand and contract as stem cell loss is compensated by the proliferation of neighbors (Lopez-Garcia et al., 2010; Snippert et al., 2010). Notably, we observed that the numbers of partly populated crypts remain unchanged with age, whereas wholly populated crypts accumulate at a predictable rate in $R26^{[CA]30SYNbglA}$ mice. This indicates that the de novo appearance of partly populated crypts is balanced either by loss of labeled clones or their expansion to populate whole crypts. Such behavior is predicted by neutral-drift theory.

A mathematical model was developed that accounts for the continuous appearance of newly labeled cells, as well as the subsequent neutral-drift dynamics that follow labeling (Supplemental Experimental Procedures available online). The model accurately predicts that the rate of accumulation of wholly populated crypts (ΔC_{fix}) is linear and that the frequency of transition-form clones, or partly populated crypts (C_{part}), remains constant over time. The former depends on two variables: the mutation rate of the $[CA]_{30}$ tract and the rate of stem cell replacement per crypt (λ_{crypt}). The latter depends on mutation rate and the number of stem cells per crypt (N_{crypt}). Thus, both parameters share a common dependency on mutation rate. The clone incidence data in Figures 1E–1G shows a constant relationship between fixed and transition forms, demonstrating that both the number of stem cells and their rate of replacement do not change with age.

Determining the $[CA]_{30}$ Mutation Rate

Specific values for stem cell number and replacement rate can be inferred by calculating the mutation rate of the $[CA]_{30}$ dinucleotide repeat (α). $R26^{[CA]30EYFP}$ animals with an *EYFP* reporter gene were generated and used to determine the intestinal $[CA]_{30}$ mutation rate (Supplemental Experimental Procedures and Figure S1A). Crypts transected immediately above the crypt base were scored for the presence of single or pairs of $EYFP^+$ cells (Figure 1H). Adjacent serial sections were then scored to ensure that these positive cells were not part of a larger, pre-existing clone and were therefore de novo mutations. This analysis identified 34 positive cells in 17,000 crypts scored (equating to 289,000 cells scored), allowing the in vivo rate of mutagenesis of the $[CA]_{30}$ tract to be calculated as $1.17 \times 10^{-4} \pm 0.40 \times 10^{-4}$ (95% CI) mutants per mitosis (Figure 1I and Supplemental Experimental Procedures).

In addition, the mutation rate was estimated in mouse embryonic fibroblast (MEF) cultures derived from $R26^{[CA]30EYFP}$ mice and found to be $1.06 \times 10^{-4} \pm 0.38 \times 10^{-4}$ (95% CI) mutants per mitosis (Figures 1I and S1B–S1D). Published estimates for mutation rates of similarly sized repeat tracts are consistent with those described here (Yamada et al., 2002). Cumulatively, these observations suggest that the mutation rate for a given repeat tract, in mismatch-repair-competent cells, does not vary between highly different cellular contexts.

Determining Stem Cell Number and Replacement Rate

The mutation rate was then used together with the equations that describe ΔC_{fix} and C_{part} for calculating both λ_{crypt} and N_{crypt}. This analysis indicates that there are 5 ± 0.3, 6 ± 0.4, and 7 ± 0.3 (95% CI) stem cells per crypt in proximal SI, distal SI, and colon, respectively, and that the rate at which an individual stem cell is replaced per day is 0.1 ± 0.01, 0.2 ± 0.05, and 0.3 ± 0.04 (95% CI), respectively. The resulting fit overlays with the data for each region, whereas higher values for number and replacement rate do not (Figures 1E–1G and 1J). Thus, regional differences in the dynamics of neutral drift arise from differences in both the number of stem cells per crypt and the rate at which they are replaced.

Reconciliation with Pulse-Chase Analyses

Strikingly, these estimates suggest both lower numbers of stem cells per crypt and rates of stem cell replacement compared to those derived using pulse-chase labeling (16 stem cells;

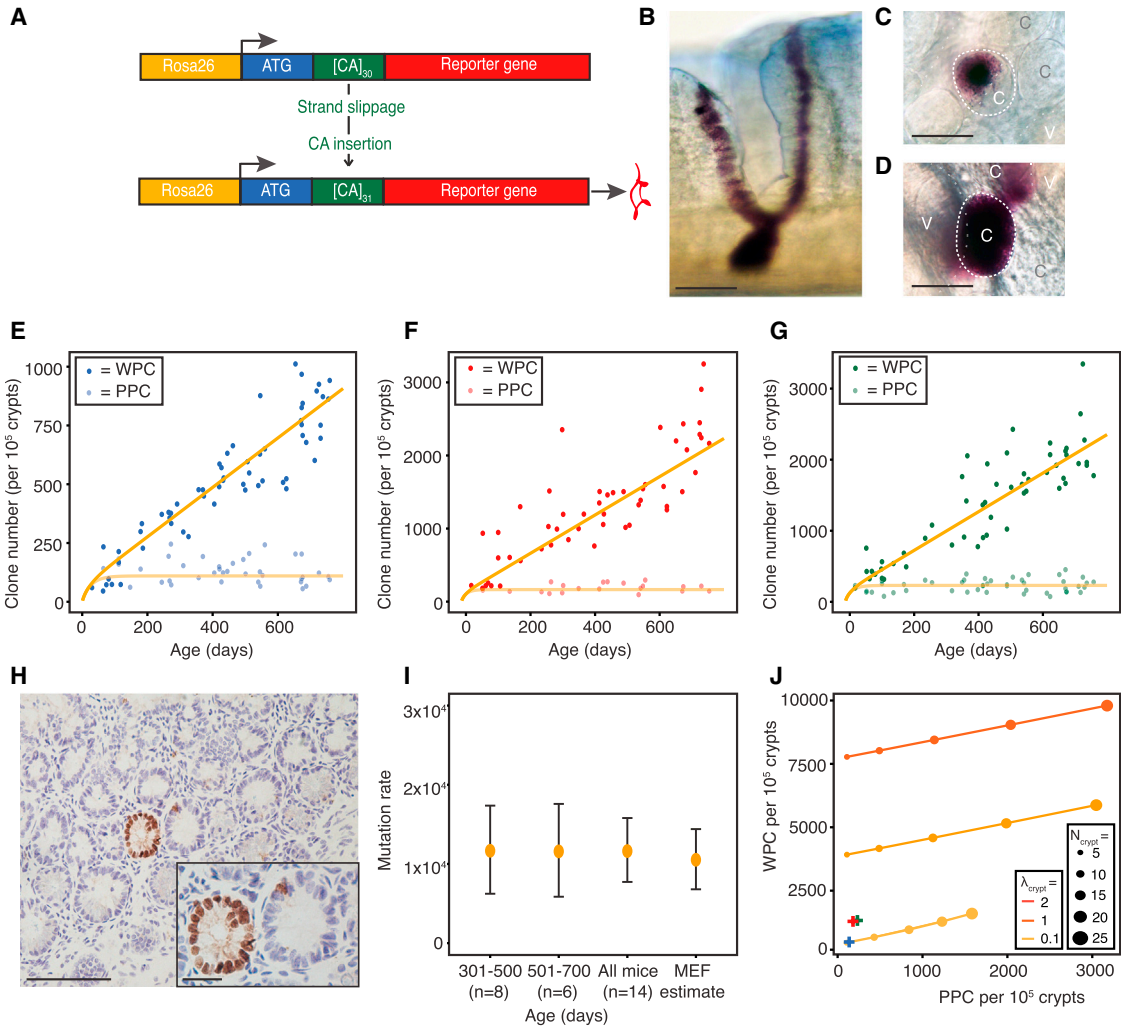

Figure 1. Clone Data Acquired Using the R26$^{[CA]30}$ Continuous-Labeling Strategy

(A) *R26$^{[CA]30}$* mice contain a $[CA]_{30}$ dinucleotide repeat and a reporter gene, either *SYNbglA* or *EYFP*, targeted to the Rosa26 locus. When the repeat tract is intact ($[CA]_{30}$) the reporter gene is out of frame. If strand slippage occurs during DNA replication, the insertion of one CA will push the reporter gene in-frame, leading to translation of a fully functional protein.

(B) Representative image of a fully labeled crypt in the distal SI, lightly counterstained with Alcian blue (scale bar represents 25 μm).

(C and D) Representative images of whole-mounted tissue showing partly (C) or wholly (D) populated crypts in the proximal SI. Crypts are denoted with a "c," a dashed line indicates the labeled crypt boundary, and dotted lines encircle villi (v) out of the focal plane. Scale bars represent 25 μm.

(E–G) Scatter plots showing the number of partly populated crypts (PPC) and wholly populated crypts (WPC) in the proximal SI (E), distal SI (F), and colon (G). In all three regions the number of partly populated crypts remains stable with age, whereas the number of wholly populated crypts increases linearly with age. The age-related behavior of wholly populated and partly populated crypts as predicted by neutral drift overlays with the data observed in vivo in the proximal SI (E), distal SI (F), and colon (G). The orange lines indicate the theoretical prediction of the data when $\alpha = 1.1 \times 10^{-4}$.

(H) EYFP immunohistochemistry in *en face* sections of SI tissue taken from *R26$^{[CA]30EYFP}$* mice and showing a crypt containing a single positive cell next to a wholly stained crypt. The inset shows an enlargement of the area (scale bars represent 50 μm).

(I) Graph showing the mutation rate of the $[CA]_{30}$ tract obtained in vivo from *en face* sections of *R26$^{[CA]30EYFP}$* SI tissue and in vitro from *R26$^{[CA]30EYFP}$*-derived MEF cultures. Data are presented with 95% CI.

(J) Theoretical predictions of the per-mouse average number of PPC versus WPC for a range of values of N_{crypt} and λ_{crypt}. Possible values of N_{crypt} are represented by circles of increasing size, whereas possible values of λ_{crypt} are represented by orange lines. The three crosses represent the data averaged over the full data set for proximal SI (blue), distal SI (red), and colon (green).

See also Figures S1 and S2.

replacement rate of 0.74–1 per stem cell per day), which assumed that the number of stem cells per crypt corresponds to the total number of crypt-base intercalated or Lgr5^{+} cells (Lopez-Garcia et al., 2010; Snippert et al., 2010). To explain this disparity, we sought to identify the optimal values for the number and replacement rate of stem cells required to generate the clone size distributions previously observed following induction pulses in the SI of *Lgr5$^{EGFP\text{-}IRES\text{-}creERT2}$/R26^{Confetti}* mice and in the colon of *Ah^{creERT}/R26^{SYNbglA}* mice (Lopez-Garcia et al., 2010; Snippert et al., 2010). The fit to the data was found

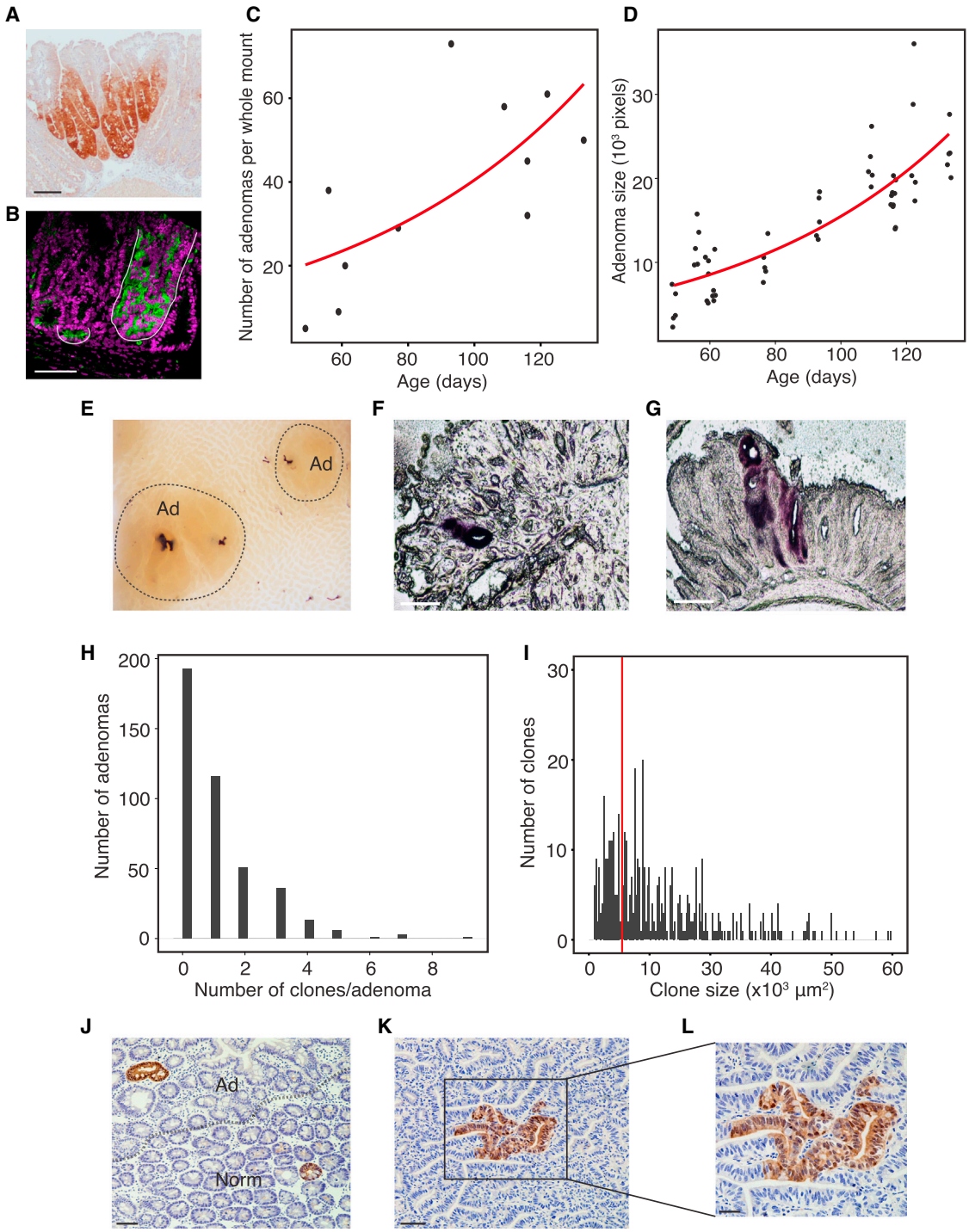

Figure 2. Growth of *Apc*^{min} Adenomas and Predicted R26$^{[CA]30}$ Clone Data

(A) Longitudinal section showing distribution of Lgr5^{+} cells in an *Apc*^{min} adenoma revealed using immunohistochemistry to EGFP (scale bar represents 50 μm).

(B) Longitudinal section showing distribution of Lgr5^{+} cells in an *Apc*^{min} adenoma and neighboring normal crypt revealed using immunofluorescence to EGFP (scale bar represents 100 μm).

(C) Quantification of the number of adenomas per whole mount ($p < 2 \times 10^{-15}$).

(D) Quantification of the size of the five largest adenomas per whole mount ($p < 2 \times 10^{-16}$).

(E) Representative image of two adenomas (Ad) from an *R26*$^{[CA]30SYNbglA}$/*Apc*^{min} whole mount with individual large SYNbglA-positive clones clearly visible.

(F and G) Adenomas isolated from *R26*$^{[CA]30SYNbglA}$/*Apc*^{min} mice contain clones as seen *en face* (F) or on edge (G) in 20 μm vibratome sections (scale bar represents 250 μm).

(H) Frequency histogram of clone incidence per adenoma.

(legend continued on next page)

to be significantly improved (based on consideration of the mean squared error) using values derived from continuous clonal labeling of six stem cells per crypt and a replacement rate of 0.2 stem cells per day in the distal SI and seven stem cells per crypt and a replacement rate of 0.3 stem cells per day in the colon, compared to those originally proposed (Figures S2A and S2C and Supplemental Experimental Procedures).

Recently it has been suggested that high doses of tamoxifen may ablate stem cells and cause a regenerative response in the intestinal epithelium (Zhu et al., 2013). To test for an effect of tamoxifen dose, we performed a similar analysis using the inducible *cre* lines $Ah^{creERT}/R26^{tdTomato}$ and $Lgr5^{EGFP\text{-}IRES\text{-}creERT2}/R26^{tdTomato}$ at greatly reduced doses of tamoxifen (0.15 mg versus the 5 mg used previously). In both cases, the resultant changes in clone-size distribution are best explained by the values for stem cell number and replacement rate derived from continuous labeling (Figures S2B and S2D and Supplemental Experimental Procedures). Taken together, these data indicate that the estimates of λ_{crypt} and N_{crypt} obtained using continuous clonal labeling are in concordance with pulse-chase data, and that clone-size distributions are not influenced by tamoxifen dose, making it unlikely that tamoxifen ablates functional stem cells.

Predictions of Neutral-Drift Theory in Apc^{min} Adenomas

Analysis by "retracing" in adenomas previously described in qualitative terms that individual $Lgr5^+$ stem cells rapidly populate adenomatous glands (Schepers et al., 2012). However, with potentially hundreds of stem cells per gland identifiable by this criterion, the actual number of clonogenic cells remains unknown. The cellular content of transformed glands from ten $Lgr5^{EGFP\text{-}IRES\text{-}creERT2}/Apc^{min}$ tumors was estimated from longitudinal histological sections at 1,906 cells ± 396 (95% CI). Individual tumors were analyzed for $EGFP^+$ cells using immunofluorescence and immunohistochemistry. Immunoreactivity was extensive and extended from the base to the upper half of glands, suggesting that the $Lgr5^+$ population must be on the order of several hundred per gland (Figures 2A and 2B). This finding was confirmed by quantification of $Lgr5^{hi}$-expressing cells in $Lgr5^{EGFP\text{-}IREScreERT2}/R26^{tdTomato}/Apc^{lx/lx}$ mice following *Apc* deletion that indicated that around 20% of cells in an adenomatous gland (equating to ~400 cells) express *Lgr5* (Figures S3A and S3B). This motivated us to consider applying continuous labeling to determine stem cell numbers and rates of replacement following neoplastic transformation.

In Apc^{min} mice, intestinal adenoma development proceeds during adult life because of an inactivating germline mutation of *Apc*. Cohorts of $R26^{[CA]30SYNbglA}/Apc^{min}$ mice were aged, and animals were killed for clone detection between 41 and 200 days of age. Visual inspection confirmed the presence of adenomas. A computational analysis of digitized images of whole mounts was undertaken using a custom-built automated algorithm for adenoma (and subsequent clone) recognition (Figure S3C and Supplemental Experimental Procedures). The analysis identified 411 adenomas in 11 animals and confirmed that both adenoma number and size increase with age (Figures 2C and 2D). To accurately quantify the growth of adenomas, the five largest adenomas per whole mount were selected as being the most established and probable to have been present throughout adult life. Apc^{min} adenomas are known to grow through the process of gland fission (Wasan et al., 1998). Using the average gland size and the size of each adenoma, we were able to calculate an adenoma growth rate of approximately six glands per day (Figures S3D–S3F). This growth rate was then used to determine the estimated age (in days) of each adenoma analyzed.

Clonal Patterns in $R26^{[CA]30SYNbglA}/Apc^{min}$ Adenomas

Visual inspection of $R26^{[CA]30SYNbglA}/Apc^{min}$ whole mounts confirmed that a substantial proportion of adenomas contained contiguous clones. Importantly, clones occupied only a proportion of the adenoma mass, indicating that the $[CA]_{30}$ mutations had occurred within the developing tumor (Figure 2E). A proportion of clone-bearing adenomas from $R26^{[CA]30SYNbglA}/Apc^{min}$ mice were excised and sectioned *en face* and on edge, and the staining patterns were analyzed to establish that glands orientate vertically along the same axis as that of normal crypts and that clones typically occupy one or more glands (Figures 2F and 2G). This confirmed that two-dimensional (2D) area measurements, by capturing the glandular content of adenomas, accurately quantified the size of clones. The computational analysis of digitized images of whole mounts from $R26^{[CA]30SYNbglA}/Apc^{min}$ mice was extended to include clone recognition. This analysis established that 222 of 411 adenomas in 11 animals contained clones (Figure 2H and Supplemental Experimental Procedures).

Application of Neutral-Drift Theory to $R26^{[CA]30SYNbglA}/Apc^{min}$ Adenomas

Notably, the image analysis provides two pieces of information: clone size and clone incidence. The distribution of observed clone sizes within an Apc^{min} adenoma is broad. Of the 474 clones analyzed, over 70% were larger than the average gland size (Figure 2I). Very small clones were not observed macroscopically in the whole mounts or microscopically in histological-tissue sections of the adenomas. A 2D analysis of EYFP-positive clones from $R26^{[CA]30EYFP}/Apc^{min}$ mice confirmed the observation of small numbers of large, contiguous clones (Figures 2J–2L).

We then adapted the mathematical model described above to predict the clone-size distributions for specific values of the number of stem cells per adenomatous gland (N_{gland}) and the rate of stem cell replacement (λ_{gland}) (Supplemental Experimental Procedures). When values for N_{gland} are low (e.g., N_{gland} = 10), the resulting clones are predicted to be rare and large in size. This is in striking contrast to situations wherein values for N_{gland} are high (e.g., N_{gland} = 50), which, regardless of the value of λ_{gland}, should result in a large number of small

(I) Quantification of the observed clone-size distribution within adenomas. The red line denotes the average gland size.
(J–L) Representative images of $EYFP^+$ clones within adenomas taken from $R26^{[CA]30EYFP}/Apc^{min}$ whole mounts (scale bar represents 100 μm). In (J) a region of adenoma (Ad) is visible next to adjacent normal (Norm) tissue. In (K) a large clone occupies multiple glands. (L) shows a magnified view.
See also Figure S3.

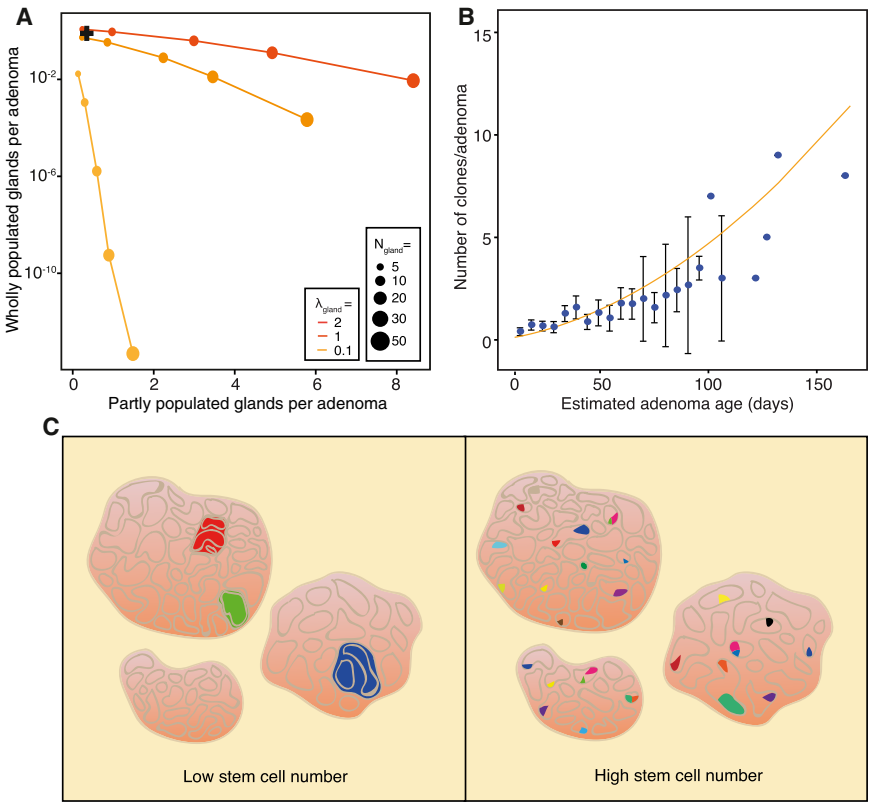

Figure 3. Application of the Continuous Clonal Label to *Apc*^{min} Adenomas

(A) Theoretical predictions of the per-adenoma average number of partly populated versus wholly populated glands for a range of values of N_{gland} and λ_{gland}. Possible values of if N_{gland} are represented by circles of increasing size, whereas possible values of λ_{gland} are represented by orange lines. The black cross represents the data averaged over all adenomas.

(B) Quantification of the number of individual clones per *R26*$^{[CA]30SYNbglA}$/*Apc*^{min} adenoma plotted against age. Bayesian inference predicts that N_{gland} = 9 and λ_{gland} = 1 (yellow line). Data are presented as the mean ± SEM.

(C) Schematic representation of the intratumoral clonal patterns expected for low (left panel) and high (right panel) numbers of stem cells. The former model is supported by the data presented. See also Figure S3.

clones (Figure 3A). These predictions suggest that small numbers of large clones in adenomas are the result of a small number of stem cells per gland.

Precise values of N_{gland} and λ_{gland} were calculated using Bayesian inference from the clone-incidence data (Supplemental Experimental Procedures). This model predicts that N_{gland} = 9 (99% CI between 8 and 9) and λ_{gland} = 1 (99% CI between 0.85 and 1.17) and provides a good fit to the observed clone-incidence data (Figure 3B). When the clone-size data for intratumor clones are considered (as large and small clones, greater or less than the mean gland size, respectively), the data are consistent with that predicted for this low value of N_{gland} (Figure 3A). These data confirm the hypothesis that clones observed in adenomas are the result of a small number of stem cells per gland (Figure 3C).

DISCUSSION

We have described a clonal-labeling approach that allows intestinal stem cells to be retrospectively analyzed over the lifetime of the organism. Strikingly, continuous clonal labeling demonstrates that previous inferences of stem numbers and replacement rates derived from pulse-chase labeling are overestimates. The explanation is surprisingly simple: the dynamics governing changes in clone size have been wrongly assumed to arise from the behavior of all cells in a given population rather than only a subset.

In other stem cell systems, there is evidence of stem cell exhaustion in aging animals (Chambers et al., 2007; Pietras et al., 2011). In hematopoiesis, this manifests as an increase in the number of phenotypic stem cells that are functionally impaired in respect to being able to support multilineage reconstitution on transplantation and in the number of cell divisions they can undergo (Rossi et al., 2005; Janzen et al., 2006; Nygren and Bryder, 2008). We have shown that both the number of intestinal stem cells and their rate of replacement are unchanging up to at least 2 years of age, and therefore we find no evidence for the exhaustion of intestinal stem cells during adult life.

The precise identity of the stem cells maintaining the intestinal epithelium has been much debated, with alternative views either supporting the Lgr5^{+} intercalated cells of the crypt base or the supra-Paneth cells that express markers such as *Hopx*. Recent attempts to resolve this debate have focused on the overlap in expression between the populations (Itzkovitz et al., 2012; Muñoz et al., 2012). This appears to suggest that *Lgr5* expression defines all putative stem populations and cell locations. Establishing that only a proportion (30%–50%) of the lower crypt population act as the de facto stem cells raises the possibility that such cells may require the expression of other factors in addition to *Lgr5*. Alternatively, *Lgr5* expression may be sufficient for stem cell potential, but redundancy within the population may mean that only a proportion actually achieves it.

The consequences of both reduced numbers of stem cells and the rates of stem cell replacement observed here are profound. It was previously estimated that a stem cell replaced its neighbor once every 32 hr, approximating to the 24 hr cell-cycle time of crypt-base cells (Snippert et al., 2010). Our revised parameters show this to be once every 5 or 10 days for proximal and distal SI, respectively, suggesting that there are more divisions than stem cell replacement events. These additional stem cell divisions probably reflect asymmetric fates for their daughters.

Interpretation of continuous-labeling data requires an estimate of mutation rate that might be predicted to vary with different tissue contexts. However, we find that this is not the case by

observing very similar rates in fibroblasts in vitro and proliferative epithelial cells in vivo, suggesting that other factors such as chromatin context may be more relevant than tissue context in determining the susceptibility of the locus to mutation.

Continuous labeling has the advantage of not requiring an experimental intervention to induce Cre-mediated recombination. Recently, it has been proposed that tamoxifen treatment, common to pulse-chase experiments, effectively ablates cells, and that some or all of the subsequent inferences are influenced by regenerative effects (Zhu et al., 2013). Comparison of our own (low-dose) pulse-chase clone data with that published following a high-dose protocol identifies no obvious effect over a 30-fold dosing range. The consistency of our estimates of stem cell number and rate of replacement using both continuous and pulse-chase labeling demonstrates that the effect of tamoxifen toxicity is minimal.

The widespread expression of *Lgr5* in adenomas suggests a potential population of several hundred stem cells in each adenomatous gland (Schepers et al., 2012). However continuous clonal labeling identifies much smaller numbers of working stem cells. Given that vertical cellular migration in adenomas has been described previously, it appears that most of the $Lgr5^{+}$ population is not part of a stable stem cell zone but rather that they actively migrate (Wong et al., 2002). Within this arrangement, only the progeny of stem cells situated toward the base of glands are retained. Furthermore, unlike homeostasis, the replacement rate of this small number of stem cells (100% replaced per day) closely approximates the cell-cycle time, requiring all adenoma stem cell divisions to be symmetric and leading to replacement of or by neighbors.

It is implicit in the CSC hypothesis that following oncogenic transformation a higher proportion of stem cell divisions will be self-renewing and that this drives adenoma growth. Here, we show that this process is remarkably inefficient. For example, in an adenoma comprised of 100 adenomatous glands (with nine stem cells per gland), of the 900 stem cell-renewal events per day, around 850 will be to replace existing stem cells and only 50 will contribute to the growth of the tumor. Thus, the majority of self-renewing divisions act to replace stem cells lost from the adenoma presumably due to either commitment or cell death. The net effect of this organization is that clones inevitably populate intratumoral territories maintained by a common stem cell pool. It follows that the bulk of tumor stem cells are primed for displacement and eventual extinction and that drugs enhancing this predisposition may form the basis for novel therapies.

EXPERIMENTAL PROCEDURES

Genetically Modified Animals

The $R26^{[CA]30SYNbglA}$ and $R26^{[CA]30EYFP}$ strains have not been previously described. In brief, $[CA_{30}]$-*SYNBglA* and $[CA_{30}]$-*EYFP* reporter cassettes were synthesized by Yorkshire Bioscience. These were subsequently subcloned by Nhe1 digestion into the pROSA-MCS13-puro targeting construct (Vooijs et al., 2001). Gene targeting was carried out by the transgenic facility at the Cancer Research UK London Research Institute in an embryonic stem cell line of C57Bl/6 genetic background (cell line: B6 1.1). $R26^{[CA]30SYNbglA}$ and $R26^{[CA]30EYFP}$ mice were subsequently maintained as hemizygotes on a C57Bl/6J genetic background. $R26^{[CA]30SYNbglA}$ and $R26^{[CA]30EYFP}$ mice were crossed with Apc^{min} mice (Jackson Laboratory, stock number: 002020). Animals carrying both alleles were selected for further analysis and maintained on a C57Bl/6J background. All animals were cared for at the Cancer Research UK Cambridge Institute Biological Resources Unit according to Home Office regulations.

Whole-Mount Staining and Clone Scoring

Detection of *SYNbglA* expression was carried out as previously described (Lopez-Garcia et al., 2010; McCutcheon et al., 2010).

Image Analysis

Tessellate photographs of $R26^{[CA]30SYNbglA}/Apc^{min}$ whole mounts were taken on a dissecting microscope (Wild Heerbrugg M8) with additional incidental lighting. Images were digitally stitched together to create a single image file of each whole mount. This image was computationally analyzed (Supplemental Experimental Procedures) for detection of the tissue, pins, clones, and adenomas. Subsequently, the area of individual clones and adenomas was quantified in relation to a known size marker. This size in metric units was then translated to a size in glands. To calculate the average size of a gland within an Apc^{min} adenoma, hematoxylin and eosin-stained *en face* paraffin sections were taken from ten adenomas. The tissue sections were then photographed (Leica DMI6000 B), and the sizes of 903 glands were quantified in ImageJ (http://rsbweb.nih.gov/ij/).

SUPPLEMENTAL INFORMATION

Supplemental Information includes three figures and Supplemental Experimental Procedures and can be found with this article online at http://dx.doi.org/10.1016/j.stem.2013.08.001.

ACKNOWLEDGMENTS

This work was supported by Cancer Research UK, and L.V. is the recipient of a KWF fellowship from the Dutch Cancer Society. We gratefully acknowledge the following core facilities at the Cancer Research UK Cambridge Institute: the Transgenic Laboratory, the Biological Resources Unit, and Histopathology.

Received: February 12, 2013
Revised: July 12, 2013
Accepted: August 7, 2013
Published: September 12, 2013

REFERENCES

Barker, N., van Es, J.H., Kuipers, J., Kujala, P., van den Born, M., Cozijnsen, M., Haegebarth, A., Korving, J., Begthel, H., Peters, P.J., and Clevers, H. (2007). Identification of stem cells in small intestine and colon by marker gene Lgr5. Nature *449*, 1003–1007.

Chambers, S.M., Shaw, C.A., Gatza, C., Fisk, C.J., Donehower, L.A., and Goodell, M.A. (2007). Aging hematopoietic stem cells decline in function and exhibit epigenetic dysregulation. PLoS Biol. *5*, e201.

Humphries, A., Cereser, B., Gay, L.J., Miller, D.S., Das, B., Gutteridge, A., Elia, G., Nye, E., Jeffery, R., Poulsom, R., et al. (2013). Lineage tracing reveals multipotent stem cells maintain human adenomas and the pattern of clonal expansion in tumor evolution. Proc. Natl. Acad. Sci. USA *110*, E2490–E2499.

Itzkovitz, S., Lyubimova, A., Blat, I.C., Maynard, M., van Es, J., Lees, J., Jacks, T., Clevers, H., and van Oudenaarden, A. (2012). Single-molecule transcript counting of stem-cell markers in the mouse intestine. Nat. Cell Biol. *14*, 106–114.

Janzen, V., Forkert, R., Fleming, H.E., Saito, Y., Waring, M.T., Dombkowski, D.M., Cheng, T., DePinho, R.A., Sharpless, N.E., and Scadden, D.T. (2006). Stem-cell ageing modified by the cyclin-dependent kinase inhibitor p16INK4a. Nature *443*, 421–426.

Lopez-Garcia, C., Klein, A.M., Simons, B.D., and Winton, D.J. (2010). Intestinal stem cell replacement follows a pattern of neutral drift. Science *330*, 822–825.

McCutcheon, S.C., Jones, K., Cumming, S.A., Kemp, R., Ireland-Zecchini, H., Saunders, J.C., Houghton, C.A., Howard, L.A., and Winton, D.J. (2010). Characterization of a heat resistant beta-glucosidase as a new reporter in cells and mice. BMC Biol. *8*, 89.

Montgomery, R.K., Carlone, D.L., Richmond, C.A., Farilla, L., Kranendonk, M.E., Henderson, D.E., Baffour-Awuah, N.Y., Ambruzs, D.M., Fogli, L.K., Algra, S., and Breault, D.T. (2011). Mouse telomerase reverse transcriptase (mTert) expression marks slowly cycling intestinal stem cells. Proc. Natl. Acad. Sci. USA *108*, 179–184.

Muñoz, J., Stange, D.E., Schepers, A.G., van de Wetering, M., Koo, B.K., Itzkovitz, S., Volckmann, R., Kung, K.S., Koster, J., Radulescu, S., et al. (2012). The Lgr5 intestinal stem cell signature: robust expression of proposed quiescent '+4' cell markers. EMBO J. *31*, 3079–3091.

Nygren, J.M., and Bryder, D. (2008). A novel assay to trace proliferation history in vivo reveals that enhanced divisional kinetics accompany loss of hematopoietic stem cell self-renewal. PLoS ONE *3*, e3710.

O'Brien, C.A., Pollett, A., Gallinger, S., and Dick, J.E. (2007). A human colon cancer cell capable of initiating tumour growth in immunodeficient mice. Nature *445*, 106–110.

Pietras, E.M., Warr, M.R., and Passegué, E. (2011). Cell cycle regulation in hematopoietic stem cells. J. Cell Biol. *195*, 709–720.

Reizel, Y., Chapal-Ilani, N., Adar, R., Itzkovitz, S., Elbaz, J., Maruvka, Y.E., Segev, E., Shlush, L.I., Dekel, N., and Shapiro, E. (2011). Colon stem cell and crypt dynamics exposed by cell lineage reconstruction. PLoS Genet. *7*, e1002192.

Rossi, D.J., Bryder, D., Zahn, J.M., Ahlenius, H., Sonu, R., Wagers, A.J., and Weissman, I.L. (2005). Cell intrinsic alterations underlie hematopoietic stem cell aging. Proc. Natl. Acad. Sci. USA *102*, 9194–9199.

Sangiorgi, E., and Capecchi, M.R. (2008). Bmi1 is expressed in vivo in intestinal stem cells. Nat. Genet. *40*, 915–920.

Schepers, A.G., Snippert, H.J., Stange, D.E., van den Born, M., van Es, J.H., van de Wetering, M., and Clevers, H. (2012). Lineage tracing reveals Lgr5+ stem cell activity in mouse intestinal adenomas. Science *337*, 730–735.

Shackleton, M., Quintana, E., Fearon, E.R., and Morrison, S.J. (2009). Heterogeneity in cancer: cancer stem cells versus clonal evolution. Cell *138*, 822–829.

Shmelkov, S.V., Butler, J.M., Hooper, A.T., Hormigo, A., Kushner, J., Milde, T., St Clair, R., Baljevic, M., White, I., Jin, D.K., et al. (2008). CD133 expression is not restricted to stem cells, and both CD133+ and CD133- metastatic colon cancer cells initiate tumors. J. Clin. Invest. *118*, 2111–2120.

Siminovitch, L., McCulloch, E.A., and Till, J.E. (1963). The Distribution of Colony-Forming Cells among Spleen Colonies. J. Cell. Physiol. *62*, 327–336.

Snippert, H.J., van der Flier, L.G., Sato, T., van Es, J.H., van den Born, M., Kroon-Veenboer, C., Barker, N., Klein, A.M., van Rheenen, J., Simons, B.D., and Clevers, H. (2010). Intestinal crypt homeostasis results from neutral competition between symmetrically dividing Lgr5 stem cells. Cell *143*, 134–144.

Takeda, N., Jain, R., LeBoeuf, M.R., Wang, Q., Lu, M.M., and Epstein, J.A. (2011). Interconversion between intestinal stem cell populations in distinct niches. Science *334*, 1420–1424.

Till, J.E., and McCulloch, E.A. (1961). A direct measurement of the radiation sensitivity of normal mouse bone marrow cells. Radiat. Res. *14*, 213–222.

Vooijs, M., Jonkers, J., and Berns, A. (2001). A highly efficient ligand-regulated Cre recombinase mouse line shows that LoxP recombination is position dependent. EMBO Rep. *2*, 292–297.

Wasan, H.S., Park, H.S., Liu, K.C., Mandir, N.K., Winnett, A., Sasieni, P., Bodmer, W.F., Goodlad, R.A., and Wright, N.A. (1998). APC in the regulation of intestinal crypt fission. J. Pathol. *185*, 246–255.

Winton, D.J., and Ponder, B.A. (1990). Stem-cell organization in mouse small intestine. Proc. Biol. Sci. *241*, 13–18.

Winton, D.J., Blount, M.A., and Ponder, B.A. (1988). A clonal marker induced by mutation in mouse intestinal epithelium. Nature *333*, 463–466.

Wong, W.M., Mandir, N., Goodlad, R.A., Wong, B.C., Garcia, S.B., Lam, S.K., and Wright, N.A. (2002). Histogenesis of human colorectal adenomas and hyperplastic polyps: the role of cell proliferation and crypt fission. Gut *50*, 212–217.

Yamada, N.A., Smith, G.A., Castro, A., Roques, C.N., Boyer, J.C., and Farber, R.A. (2002). Relative rates of insertion and deletion mutations in dinucleotide repeats of various lengths in mismatch repair proficient mouse and mismatch repair deficient human cells. Mutat. Res. *499*, 213–225.

Zhu, Y., Huang, Y.F., Kek, C., and Bulavin, D.V. (2013). Apoptosis differently affects lineage tracing of Lgr5 and Bmi1 intestinal stem cell populations. Cell Stem Cell *12*, 298–303.